Guiding cold atoms in a hollow laser beam

Xinye Xu,[1,2] V. G. Minogin,[1,3] Kwanil Lee,[1] Yuzhu Wang,[2] and Wonho Jhe[1]*
[1]*Center for Near-field Atom-photon Technology and Department of Physics, Seoul National University, Seoul 151-742, Korea*
[2]*Laboratory for Quantum Optics, Shanghai Institute of Optics and Fine Mechanics, Chinese Academy of Sciences, Shanghai 201800, China*
[3]*Institute of Spectroscopy, Russian Academy of Sciences, 142092, Troitsk, Moscow Region, Russia*
(Received 23 June 1999)

The theory of atom guiding in a far blue-detuned hollow laser beam (HLB) is developed for the dipole interaction scheme described by a three-level Λ model. The complete kinetic description of atomic motion based on the Fokker-Planck equation for the atomic distribution function is presented. The dipole gradient force, radiation pressure force, and momentum diffusion tensor are then derived. It is found that even for a far-detuned laser beam, the optical potential for a three-level Λ atom is not generally reduced to a sum of two independent potentials associated with the two two-level interactions in the Λ scheme. The theory developed here is also compared with the experimental guiding of cold ^{85}Rb atoms in the HLB. The experimental results are found to be in good agreement with the Monte Carlo simulations based on the three-level Λ model. We observe that the guiding efficiency depends strongly on the intensity and the detuning of the HLB and the initial temperature of atoms. In particular, the experimental results show that, at small detunings, the guiding efficiency is deteriorated strongly by the radiation pressure force. The Monte Carlo simulations also indicate that the efficiency of guiding versus detuning depends strongly on the direction of the HLB propagation with respect to that of atomic motion. Under optimal conditions, the guiding efficiency was found to be about 20%. [S1050-2947(99)09112-X]

PACS number(s): 32.80.Pj, 32.80.Lg, 39.10.+j, 42.50.Vk

I. INTRODUCTION

During the past several years, there has been a growing interest in the guiding of atoms in the evanescent waves developed inside hollow optical fibers (HOFs) [1–12], in the optical dipole potentials due to hollow laser beams (HLBs) [13–21], and in the use of the optical dipole potentials in optical or gravito-optical traps [13,14]. The development of an efficient atomic guiding coupler is of importance for the applications related to the transfer of cold atoms from an atom trap, such as the magneto-optical trap (MOT), to the spatial regions where atoms can be experimentally used for different applications, such as Bose condensation, high-resolution spectroscopy, and atom optics. On the other hand, there are still some unclear basic questions associated with the efficiency of atomic guiding in the optical dipole potential. For example, the basic questions on the optimal value of the laser beam detuning and the influence of the radiation pressure force on the atomic velocity distribution remain unaddressed.

The present paper is devoted to the analysis of the efficiency of atomic guiding in the HLB for a case of ^{85}Rb atoms. We present a theoretical analysis of atom guiding for a practically important model of a three-level Λ atom interacting with a far blue-detuned HLB and describe an experiment on guiding ^{85}Rb atoms from the MOT to the observation region located 11 cm below the MOT center.

Our experimental results show that in the case of cold atoms released from the MOT and falling freely under the gravity force in the guiding potential, the guiding efficiency depends strongly on the direction of the guiding-laser propagation with respect to the direction of guided atoms due to the contribution of the radiation pressure force. In principle, the contribution of the radiation pressure force could be reduced by choosing a relatively large value of the detuning. In any practical guiding scheme, however, the increase of the detuning is accompanied by the decreases of the effective saturation, and consequently the height of the guiding potential becomes decreased. Any compromise between the necessity of choosing a relatively large detuning and of simultaneously keeping the saturation at a proper level results in the unavoidable presence of the radiation pressure force.

When the HLB propagates counter to the guiding direction of atoms, the radiation pressure force decelerates the atoms and even reverses the velocities of the slowly moving atoms. As a result, the flux of guided atoms and accordingly the guiding efficiency are decreased. We conclude at this point that, for the counterpropagating direction of the HLB with respect to the atomic guiding, the contribution of the radiation pressure force is the main cause that limits the guiding efficiency at intermediate detunings. At large detunings, on the other hand, the contribution of the radiation pressure force can be negligibly small, but the height of the potential barrier also becomes small.

In Sec. II, the basic microscopic equations describing the interaction of a three-level Λ atom with a single-mode laser wave are presented. Section III is devoted to the derivation of the radiation pressure force and momentum diffusion tensor for a chosen interaction scheme. In Sec. IV, the dipole gradient force and the optical dipole potential are derived. Sec. V presents the radiation forces, optical dipole potential, and diffusion tensor for a specific case of a blue-detuned

*Author to whom correspondence should be addressed.
Electronic address: whjhe@phya.snu.ac.kr

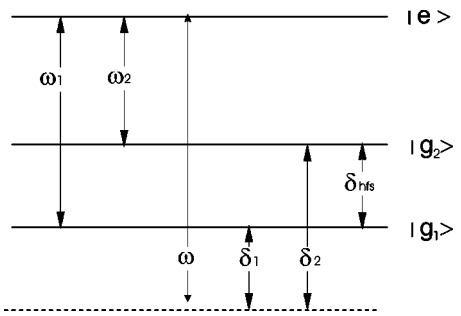

FIG. 1. Energy-level diagram of a three-level Λ atom interacting with a far-detuned single-mode laser beam.

HLB and slowly moving atoms. In Sec. VI, we discuss the dipole potential and the dipole gradient force in a simplified dressed-atom picture and compare the results with those derived from an *ab initio* analysis. Section VII describes the experimental setup used for the guiding rubidium atoms. Section VIII presents a comparison of the developed theory with the experimental data for guiding rubidium atoms in the HLB and presents the results of the Monte Carlo simulation for the guiding efficiency.

II. THREE-LEVEL INTERACTION MODEL

We consider a three-level Λ atom that includes two hyperfine-structure ground states, $|g_1\rangle=|1\rangle$ and $|g_2\rangle=|2\rangle$ and one excited state $|e\rangle=|3\rangle$, as shown in Fig. 1. An atom is assumed to interact with a single-mode traveling laser wave of frequency ω. The detunings of the laser wave with respect to the resonant transitions are $\delta_j=\omega-\omega_j$ $(j=1,2)$, where $\omega_1(\omega_2)$ is the atomic transition frequency between the ground state $|1\rangle(|2\rangle)$ and the upper state $|3\rangle$. The hyperfine structure splitting between two ground-state levels is denoted as $\delta_{hfs}=\omega_1-\omega_2$.

For the above interaction scheme, the atomic Hamiltonian can be written as

$$H=H_0-\frac{\hbar^2}{2M}\nabla^2-\mathbf{D}\cdot\mathbf{E}, \tag{1}$$

where the Hamiltonian H_0 describes the atomic energy levels E_1,E_2,E_3 and the last term describes the dipole interaction between the atom and the laser field. In our model, the laser field is chosen as a spatially inhomogeneous monochromatic laser wave,

$$\mathbf{E}=\mathbf{E}_0\cos(\mathbf{k}\cdot\mathbf{r}-\omega t), \tag{2}$$

where $\mathbf{E}_0=\mathbf{E}_0(\mathbf{r})$ is the coordinate-dependent amplitude of the laser wave and $k=\omega/c$ is the magnitude of the wave vector. Note that in the following analysis the spatially inhomogeneous phase is neglected in Eq. (2).

For a chosen three-level Λ-model scheme, the complete description of the time evolution of an atom can be given by the equations for the atomic density matrix in the Wigner representation. The dipole interaction of an atom with the laser field is considered as usual in the rotating-wave approximation (RWA) [23]. To simplify the derivation of the equations of motion, we first write the initial microscopic equations, neglecting the spatial variation of the laser beam amplitude $\mathbf{E}_0$. For the case of the laser wave (2) having a constant amplitude, the density matrix equations are obtained as

$$\begin{aligned}
\frac{d}{dt}\rho_{33}&=i\kappa_1(e^{i(\mathbf{k}\cdot\mathbf{r}-\delta_1 t)}\rho_{13}^{(-)}-e^{-i(\mathbf{k}\cdot\mathbf{r}-\delta_1 t)}\rho_{31}^{(-)})\\
&\quad+i\kappa_2(e^{i(\mathbf{k}\cdot\mathbf{r}-\delta_2 t)}\rho_{23}^{(-)}-e^{-i(\mathbf{k}\cdot\mathbf{r}-\delta_2 t)}\rho_{32}^{(-)})\\
&\quad-2(\gamma_1+\gamma_2)\rho_{33},\\
\frac{d}{dt}\rho_{22}&=i\kappa_2(e^{-i(\mathbf{k}\cdot\mathbf{r}-\delta_2 t)}\rho_{32}^{(+)}-e^{i(\mathbf{k}\cdot\mathbf{r}-\delta_2 t)}\rho_{23}^{(+)})\\
&\quad+2\gamma_2\int\Phi(\mathbf{n})\rho_{33}^{(\mathbf{n})}d^2n,\\
\frac{d}{dt}\rho_{11}&=i\kappa_1(e^{-i(\mathbf{k}\cdot\mathbf{r}-\delta_1 t)}\rho_{31}^{(+)}-e^{i(\mathbf{k}\cdot\mathbf{r}-\delta_1 t)}\rho_{13}^{(+)})\\
&\quad+2\gamma_1\int\Phi(\mathbf{n})\rho_{33}^{(\mathbf{n})}d^2n,
\end{aligned} \tag{3}$$

$$\begin{aligned}
\frac{d}{dt}\rho_{31}&=i\kappa_1 e^{i(\mathbf{k}\cdot\mathbf{r}-\delta_1 t)}(\rho_{11}^{(-)}-\rho_{33}^{(+)})+i\kappa_2 e^{i(\mathbf{k}\cdot\mathbf{r}-\delta_2 t)}\rho_{21}^{(-)}\\
&\quad-(\gamma_1+\gamma_2)\rho_{31},\\
\frac{d}{dt}\rho_{32}&=i\kappa_2 e^{i(\mathbf{k}\cdot\mathbf{r}-\delta_2 t)}(\rho_{22}^{(-)}-\rho_{33}^{(+)})+i\kappa_1 e^{i(\mathbf{k}\cdot\mathbf{r}-\delta_1 t)}\rho_{12}^{(-)}\\
&\quad-(\gamma_1+\gamma_2)\rho_{32},\\
\frac{d}{dt}\rho_{12}&=i\kappa_1 e^{-i(\mathbf{k}\cdot\mathbf{r}-\delta_1 t)}\rho_{32}^{(+)}-i\kappa_2 e^{i(\mathbf{k}\cdot\mathbf{r}-\delta_2 t)}\rho_{13}^{(+)}.
\end{aligned}$$

Here the density matrix elements are defined with respect to the time-dependent, stationary atomic eigenfunctions in a usual way,

$$\rho_{ab}^{(\pm)}=\langle a|\rho(\mathbf{r},\mathbf{p}\pm\tfrac{1}{2}\hbar\mathbf{k},t)|b\rangle,\quad \rho_{ab}^{(\mathbf{n})}=\langle a|\rho(\mathbf{r},\mathbf{p}+\mathbf{n}\hbar k,t)|b\rangle,$$

where $(a,b)=1,2,3$, $\mathbf{n}$ is a unit vector that defines the direction of the spontaneous photon emission, and the total time derivative is

$$\frac{d}{dt}=\frac{\partial}{\partial t}+\mathbf{v}\frac{\partial}{\partial\mathbf{r}}. \tag{4}$$

The halves of the Rabi frequencies κ_j and the partial spontaneous decay rates γ_j are defined as $(j=1,2)$

$$\kappa_j=\frac{\Omega_j}{2}=\frac{\mathbf{d}_{j3}\cdot\mathbf{E}_0}{2\hbar},\quad 2\gamma_j=W_{sp}^j=\frac{4}{3}\frac{d_{j3}^2\omega_0^3}{\hbar c^3}. \tag{5}$$

In Eqs. (3), the function $\Phi(\mathbf{n})$ describes the angular anisotropy of the spontaneous photon emission. In our simplified model that neglects the atomic level degeneracy, the function $\Phi(\mathbf{n})$ is chosen to be isotropic, such that

$$\Phi(\mathbf{n})=\frac{1}{4\pi},\quad\int\Phi(\mathbf{n})d^2n=1. \tag{6}$$

Note also that the microscopic equations for the considered model scheme do not include the integral term in the equation for the ground-state coherence ρ_{12}.

III. RADIATION PRESSURE FORCE AND DIFFUSION COEFFICIENT

The initial microscopic equations (3) can be reduced to a Fokker-Planck-type kinetic equation in a usual way. Eliminating explicit time and position dependence by the substitutions,

$$\rho_{31}=\sigma_{31}e^{i(\mathbf{k}\cdot\mathbf{r}-\delta_1 t)},\quad \rho_{32}=\sigma_{32}e^{i(\mathbf{k}\cdot\mathbf{r}-\delta_2 t)},$$

$$\rho_{12}=\sigma_{12}e^{i(\delta_1-\delta_2)t}=\sigma_{12}e^{-i\delta_{hfs}t},$$

we first note that, at typical values of the Rabi frequencies small compared with the hyperfine structure splitting ($\kappa_i \ll \delta_{hfs}$), the small ground-state coherence ρ_{12} can be neglected in Eqs. (3). Consequently, we obtain

$$\frac{d}{dt}\rho_{33}=iu_1(\sigma_{13}^{(-)}-\sigma_{31}^{(-)})+iu_2(\sigma_{23}^{(-)}-\sigma_{32}^{(-)})-2(\gamma_1+\gamma_2)\rho_{33},$$

$$\frac{d}{dt}\rho_{22}=iu_2(\sigma_{32}^{(+)}-\sigma_{23}^{(+)})+2\gamma_2\int\Phi(\mathbf{n})\rho_{33}^{(\mathbf{n})}d^2n,$$

$$\frac{d}{dt}\rho_{11}=iu_1(\sigma_{31}^{(+)}-\sigma_{13}^{(+)})+2\gamma_1\int\Phi(\mathbf{n})\rho_{33}^{(\mathbf{n})}d^2n, \quad (7)$$

$$\frac{d}{dt}\sigma_{31}=iu_1(\rho_{11}^{(-)}-\rho_{33}^{(+)})+[i(\delta_1-\mathbf{k}\cdot\mathbf{v})-(\gamma_1+\gamma_2)]\sigma_{31},$$

$$\frac{d}{dt}\sigma_{32}=iu_2(\rho_{22}^{(-)}-\rho_{33}^{(+)})+[i(\delta_2-\mathbf{k}\cdot\mathbf{v})-(\gamma_1+\gamma_2)]\sigma_{32}.$$

Assuming that the interaction times exceed the spontaneous decay time ($\tau_{int}\gg\tau_{sp}=1/W_{sp}$), we can expand the density-matrix elements in the powers of the photon momentum $\hbar k$. Moreover, when $\tau_{int}\gg\tau_{sp}$, the Wigner density-matrix elements become the functionals of the Wigner distribution function

$$w=w(\mathbf{r},\mathbf{p},t)=\sum\rho_{aa},\quad a=1,2,3, \quad (8)$$

so that we can introduce the following explicit functional dependence according to the structure of the expanded equations:

$$\rho_{aa}=\left(r_{aa}^0+\frac{1}{2}\hbar k r_{aa}^1+\cdots\right)w+\frac{1}{2}\hbar k(q_{aa}^1+\cdots)\frac{\partial w}{\partial p_z}+\cdots,$$

$$\sigma_{ab}=\left(s_{ab}^0+\frac{1}{2}\hbar k s_{ab}^1+\cdots\right)w+\frac{1}{2}\hbar k(t_{ab}^1+\cdots)\frac{\partial w}{\partial p_z}+\cdots, \quad (9)$$

where $r_{aa}^0, s_{ab}^0, r_{aa}^1, s_{ab}^1, \ldots, q_{aa}^1, t_{ab}^1, \ldots$, are the functions of the atomic momentum $\mathbf{p}$ or atomic velocity $\mathbf{v}=\mathbf{p}/M$ that should be determined by the solution procedure. In accordance with the definition of the Wigner distribution function (8), the unknown diagonal functions satisfy the normalization conditions

$$\sum r_{aa}^0=1,\ \sum r_{aa}^1=0,\ \sum q_{aa}^1=0,\ \ldots. \quad (10)$$

Substituting the general solution (9) into the expanded equations for the atomic density matrix elements and analyzing the expanded equations in successively increasing orders in the photon momentum $\hbar k$, we finally derive from Eqs. (7) the Fokker-Planck equation for the Wigner distribution function $w(\mathbf{r},\mathbf{p},t)$ from Eqs. (7).

To the second order in the photon momentum $\hbar k$, the equation for the distribution function $w=w(\mathbf{r},\mathbf{p},t)$ is described by a second-order Fokker-Planck kinetic equation,

$$\frac{\partial w}{\partial t}+\mathbf{v}\frac{\partial w}{\partial \mathbf{r}}=-\frac{\partial}{\partial \mathbf{p}}(\mathbf{F}w)+\sum\frac{\partial^2}{\partial p_i^2}(D_{ii}w). \quad (11)$$

For the considered case of a plane laser wave, the quantity $\mathbf{F}$ is the radiation pressure force $\mathbf{F}_{rp}$ and D_{ii} ($i=x,y,z$) is the momentum diffusion tensor. These two basic kinetic quantities are expressed by the steady-state atomic population r_{33}^0 and the optical coherences s_1 and s_2 as given in the Appendix,

$$\mathbf{F}_{rp}=\hbar\mathbf{k}(\kappa_1 s_1+\kappa_2 s_2), \quad (12)$$

$$D_{ii}=\frac{1}{3}\hbar^2k^2\gamma r_{33}^0. \quad (13)$$

Substituting the values of r_{33}^0, s_1, and s_2, one can finally obtain the explicit expressions for the radiation pressure force and momentum diffusion tensor,

$$\mathbf{F}_{rp}=\hbar\mathbf{k}\gamma\frac{L_1L_2}{\mu_1L_2+\mu_2L_1+3L_1L_2/2}, \quad (14)$$

$$D_{ii}=\frac{1}{6}\hbar^2k^2\gamma\frac{L_1L_2}{\mu_1L_2+\mu_2L_1+3L_1L_2/2}. \quad (15)$$

In the above equations, the quantities μ_j define the relative spontaneous-emission rates for the two photon-emission channels,

$$\mu_1=\frac{\gamma_1}{\gamma_1+\gamma_2},\quad \mu_2=\frac{\gamma_2}{\gamma_1+\gamma_2}. \quad (16)$$

The dimensionless Lorentzian factors L_j ($j=1,2$) define the relative strengths of the two atomic dipole transitions and G_j's are the dimensionless saturation parameters,

$$L_j=\frac{G_j}{1+(\delta_j-\mathbf{k}\cdot\mathbf{v})^2/\gamma^2},\quad G_j=\frac{2\kappa_j^2}{\gamma^2},\quad \gamma=\gamma_1+\gamma_2. \quad (17)$$

Note that the radiation pressure force, momentum diffusion tensor, and upper-state population r_{33}^0 are proportional to the saturation parameters, since all these quantities are related to the independent absorption of laser light neigbor-

ing transitions. These absorption processes depend strongly on the efficiency of the optical pumping process. If the strength of the dipole transition, say, on transition $|1\rangle - |3\rangle$, goes to zero, i.e., $G_1=0$ and $L_1=0$, all the atomic population is transferred to the state $|1\rangle$, the upper population becomes zero, and both the radiation pressure force and momentum diffusion tensor also vanish.

IV. DIPOLE GRADIENT FORCE

We now take into consideration the dipole gradient force $\mathbf{F}_{gr}$ associated with the gradient of the laser beam amplitude $\mathbf{E}_0=\mathbf{E}_0(\mathbf{r})$. The derivation of the gradient force can be done in a way that generalizes the procedure considered in the preceding section. Representing the laser amplitude in the form of the Fourier expansion,

$$\mathbf{E}_0(\mathbf{r})=(2\pi\hbar)^{-3/2}\int \mathbf{E}_0(\mathbf{q})e^{i\mathbf{q}\cdot\mathbf{r}}d^3q,$$

one should introduce into Eqs. (3) the following substitution:

$$i\kappa_j(\mathbf{r})\rho_{ab}(\mathbf{p})\rightarrow(2\pi\hbar)^{-3/2}\int i\kappa_j(\mathbf{q})e^{i\mathbf{q}\cdot\mathbf{r}}\rho_{ab}\left(\mathbf{p}+\frac{1}{2}\hbar\mathbf{q}\right)d^3q. \tag{18}$$

For a laser beam amplitude that varies in space on a scale large compared to the size of the atomic wave packet, the expansion of the density-matrix elements to first order in a small momentum $\hbar\mathbf{q}$,

$$\rho_{ab}\left(\mathbf{p}+\frac{1}{2}\hbar\mathbf{q}\right)\simeq\rho_{ab}(\mathbf{p})+\frac{1}{2}\hbar\mathbf{q}\frac{\partial}{\partial\mathbf{p}}\rho_{ab}(\mathbf{p}),$$

transforms Eq. (18), into a new one,

$$i\kappa_j(\mathbf{r})\rho_{ab}(\mathbf{p})\rightarrow i\kappa_j(\mathbf{r})\rho_{ab}(\mathbf{p})+\frac{\hbar}{2}\nabla\kappa_j(\mathbf{r})\frac{\partial}{\partial\mathbf{p}}\rho_{ab}(\mathbf{p}). \tag{19}$$

Equation (19), after being substituted into Eqs. (7), gives the total radiation force as a sum of the radiation pressure force and the dipole gradient force,

$$\mathbf{F}=\mathbf{F}_{rp}+\mathbf{F}_{gr}. \tag{20}$$

The dipole gradient force is determined by the steady-state optical coherences as

$$\mathbf{F}_{gr}=\hbar c_1\nabla\kappa_1+\hbar c_2\nabla\kappa_2. \tag{21}$$

An explicit expression for the dipole gradient force according to the Appendix is

$$\mathbf{F}_{gr}=-\frac{\hbar}{2}\frac{(\delta_1-\mathbf{k}\cdot\mathbf{v})}{1+(\delta_1-\mathbf{k}\cdot\mathbf{v})^2/\gamma^2}\frac{\mu_1L_2}{\mu_1L_2+\mu_2L_1+3L_1L_2/2}\nabla G_1 - \frac{\hbar}{2}\frac{(\delta_2-\mathbf{k}\cdot\mathbf{v})}{1+(\delta_2-\mathbf{k}\cdot\mathbf{v})^2/\gamma^2}\frac{\mu_2L_1}{\mu_1L_2+\mu_2L_1+3L_1L_2/2}\nabla G_2, \tag{22}$$

where the saturation parameters, relative decay rates, and the Lorentz factors are determined by Eqs. (5), (16), and (17).

Note that, like the radiation pressure force, the dipole gradient force also depends on the efficiency of the optical pumping process. When the strength of the dipole interaction on any one optical transition goes to zero, the dipole gradient force also goes to zero since all the atomic population is optically pumped to that ground state that is not excited by the laser light. Finally, the force in Eq. (20) should be used in the Fokker-Planck equation, Eq. (11), as a total radiation force on an atom in the considered interaction scheme.

V. FORCES, DIFFUSION TENSOR, AND OPTICAL POTENTIAL FOR COLD ATOMS IN THE HLB

The above general relations can be directly applied to a case of cold atoms guided in HLBs. In the case of a hollow laser beam, the dipole gradient force in Eq. (22) pushes cold atoms to the central hollow region at blue detunings. For large positive detunings and slowly moving atoms, the kinetic coefficients $\mathbf{F}_{rp}$, $\mathbf{F}_{gr}$, and D_{ii} can be simplified as, neglecting the small Doppler shift $\mathbf{k}\cdot\mathbf{v}$ compared with the detunings ($|\mathbf{k}\cdot\mathbf{v}|\ll\delta_1,\delta_2$),

$$\mathbf{F}_{gr}=-\frac{\hbar}{2}\frac{\mu_1\delta_1G_2\nabla G_1+\mu_2\delta_2G_1\nabla G_2}{\mu_1G_2(1+\delta_1^2/\gamma^2)+\mu_2G_1(1+\delta_2^2/\gamma^2)+3G_1G_2/2}, \tag{23}$$

$$\mathbf{F}_{rp}=\hbar\mathbf{k}\gamma\frac{G_1G_2}{\mu_1G_2(1+\delta_1^2/\gamma^2)+\mu_2G_1(1+\delta_2^2/\gamma^2)+3G_1G_2/2}, \tag{24}$$

$$D_{ii}=\frac{1}{6}\hbar^2k^2\gamma \times\frac{G_1G_2}{\mu_1G_2(1+\delta_1^2/\gamma^2)+\mu_2G_1(1+\delta_2^2/\gamma^2)+3G_1G_2/2}. \tag{25}$$

Note now that the two saturation parameters are different due to the difference in the dipole-matrix elements for the neigboring optical transitions, $G_j\sim|\mathbf{d}_{j3}\cdot\mathbf{e}|^2$, where $\mathbf{e}$ is a unit vector describing the polarization of the laser field. The difference in the spontaneous decay rates γ_j for the two decay channels is also caused by the different dipole matrix elements. For this reason, in our simplified model, the saturation parameters can be considered as proportional to the partial spontaneous decay rates and can thus be written as

$$G_1=\mu_1G,\quad G_2=\mu_2G, \tag{26}$$

where the quantities μ_j are defined by Eq. (16) and the reduced saturation parameter G is defined as

$$G=\frac{2\kappa^2}{\gamma^2}=\frac{1}{2}\left(\frac{\|d\|E_0}{\hbar\gamma}\right)^2, \tag{27}$$

and $\|d\|$ is the reduced dipole matrix element.

Under the assumption of Eq. (26) relevant to the considered model scheme, the forces and the diffusion tensor reduce to the following simple expressions:

$$\mathbf{F}_{gr}=-\frac{\hbar}{2}\frac{(\mu_1\delta_1+\mu_2\delta_2)\nabla G}{2+\delta_1^2/\gamma^2+\delta_2^2/\gamma^2+3G/2}, \tag{28}$$

$$\mathbf{F}_{rp}=\hbar\mathbf{k}\gamma\frac{G}{2+\delta_1^2/\gamma^2+\delta_2^2/\gamma^2+3G/2}, \tag{29}$$

$$D_{ii}=\frac{1}{6}\hbar^2k^2\gamma\frac{G}{2+\delta_1^2/\gamma^2+\delta_2^2/\gamma^2+3G/2}. \tag{30}$$

The last simplification can be done for a practically important case when the detunings considerably exceed both the spontaneous decay rates and the Rabi frequencies ($\gamma\ll\delta_j$ and $\kappa_j=\Omega_j/2\ll\delta_j$),

$$\mathbf{F}_{gr}=-\frac{\hbar}{2}(\mu_1\delta_1+\mu_2\delta_2)\frac{\gamma^2}{\delta_1^2+\delta_2^2}\nabla G, \tag{31}$$

$$\mathbf{F}_{rp}=\hbar\mathbf{k}\gamma\frac{G\gamma^2}{\delta_1^2+\delta_2^2}, \tag{32}$$

$$D_{ii}=\frac{1}{6}\hbar^2k^2\gamma\frac{G\gamma^2}{\delta_1^2+\delta_2^2}. \tag{33}$$

According to Eqs. (28) and (31), in the case of cold atoms, the dipole gradient force corresponds to the optical potential U_{gr}, which is given by, for a case of large detunings,

$$U_{gr}=-\int\mathbf{F}_{gr}\cdot\mathbf{dr}=\frac{1}{2}\hbar(\mu_1\delta_1+\mu_2\delta_2)\frac{\gamma^2}{\delta_1^2+\delta_2^2}G. \tag{34}$$

At large detunings, the optical potential thus has the same position dependence as the saturation parameter $G=G(\mathbf{r})$ or the intensity of the laser beam $I=I(\mathbf{r})$.

To apply the above formulas to a real experimental scheme, we finally assume that the hollow laser beam is linearly polarized, described by the intensity distribution,

$$I=I(\rho,z)=\frac{4P}{\pi w^2}\frac{\rho^2}{w^2}\exp\left(-\frac{2\rho^2}{w^2}\right),$$

$$w=w_0\sqrt{1+\zeta(z/z_R)^2},\quad z_R=\pi w_0^2/\lambda, \tag{35}$$

where P is the laser power, $w=w(z)$ and w_0 are the beam waists at the distance z and $z=0$, respectively, and z_R is the Rayleigh length. The parameters w_0 and ζ are assumed to be found from the comparison of the real intensity distribution with that described by Eq. (35). Note that at a given coordinate z the radial intensity distribution has a maximum value $I_m=2P/\pi e w^2$ at a distance $\rho_m=w/\sqrt{2}$. For the intensity distribution Eq. (35), the reduced saturation parameter is

$$G=\frac{I}{I_S}=G_0\frac{\rho^2}{w^2}\exp\left(-\frac{2\rho^2}{w^2}\right),\quad G_0=\frac{4P}{\pi w^2 I_S},\quad I_S=\frac{c\hbar^2\gamma^2}{4\pi\|d\|^2}, \tag{36}$$

where I_S is the saturation intensity.

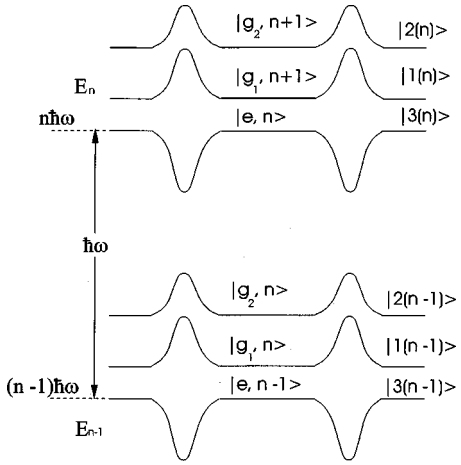

FIG. 2. Dressed states for a three-level Λ atom interacting with a hollow laser beam for positive detunings ($\delta_1,\delta_2>0$). In the zero laser field, the states of the ''atom+laser'' system are shown in the middle of the picture. The dressed states in a nonzero field are shown on the right-hand side.

VI. DRESSED ATOM PICTURE

The above *ab initio* derivation of the dipole gradient force and optical potential can also be performed by a simple qualitative picture describing the quasienergy states or the dressed states of a three-level Λ atom in the field of a laser beam (Fig. 2). In the dressed-atom representation the three bare atomic states, two ground states $|g_1\rangle=|1\rangle$ and $|g_2\rangle=|2\rangle$ and the excited state $|e\rangle=|3\rangle$, mix with the photon states $|n\rangle$ to produce three basis states $|g_1,n+1\rangle$, $|g_2,n+1\rangle$, and $|e,n\rangle$, where n is the number of photons in a laser beam. The linear superpositions of these basis states produce three dressed states $|1(n)\rangle$, $|2(n)\rangle$, and $|3(n)\rangle$ described by the eigenenergies E_{nj} $(j=1,2,3)$.

In a case of large detunings, the values of eigenenergies E_{n1} and E_{n2}, corresponding to the states $|1(n)\rangle$ and $|2(n)\rangle$, can be shown to be [22]

$$E_{nj}=n\hbar\omega+\hbar\delta_j+\hbar\frac{\kappa_j^2}{\delta_j}=n\hbar\omega+\hbar\delta_j+\frac{\hbar}{2}\frac{\mu_j\gamma^2G}{\delta_j}. \tag{37}$$

The ground-state populations, according to the Appendix, for large detunings are given by

$$r_{11}^0=\frac{\delta_1^2}{\delta_1^2+\delta_2^2},\quad r_{22}^0=\frac{\delta_2^2}{\delta_1^2+\delta_2^2}. \tag{38}$$

Accordingly, the position-dependent optical potential can be obtained as

$$U_{gr}=\frac{\hbar}{2}\left(\frac{\mu_1}{\delta_1}r_{11}^0+\frac{\mu_2}{\delta_2}r_{22}^0\right)\gamma^2G$$

$$=\frac{1}{2}\hbar(\mu_1\delta_1+\mu_2\delta_2)\frac{\gamma^2}{\delta_1^2+\delta_2^2}G. \tag{39}$$

The last expression exactly agrees with Eq. (34) derived by the strict kinetic approach.

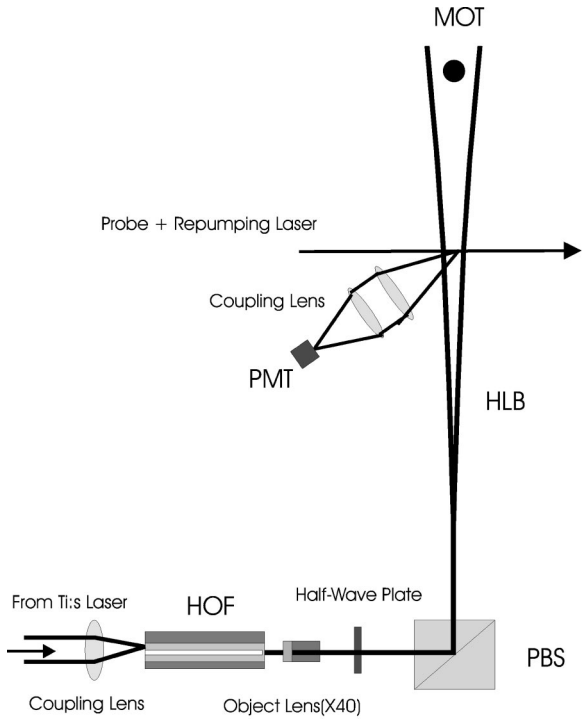

FIG. 3. Experimental setup used for guiding rubidium atoms. The hollow laser beam (HLB) produced inside the hollow optical fiber was collimated by the objective lens with a magnificaton factor of 40. The HLB was reflected by a polarization beam splitter (PBS) to propagate upward to the center of the MOT. The TOF fluorescence signal was detected by a PMT at a position 11 cm below the MOT center. The fluorescence was excited by the probe laser beam and the repumping laser beam is overlapped with the probe laser beam.

VII. EXPERIMENTAL PROCEDURES

The experimental schematic of guiding rubidium atoms is shown in Fig. 3. A hollow laser beam (HLB) was generated from a micron-sized hollow optical fiber [17] that has the inner and outer diameters of 2 μm and 6 μm, respectively. A Ti:sapphire (TS) laser pumped by an Ar-ion laser was used as the guiding laser source. The HLB used for atom guiding was chosen as being linearly polarized with the LP_{01} mode. The power of the laser mode was 180 mW. The distance between the objective lens and the MOT was 180 cm. Comparing the observed intensity distribution with that described by Eq. (35), we found the beam waist as $w_0=21$ μm and the dimensionless parameter $\zeta=0.02$.

For trapping ^{85}Rb atoms, a standard six-beam, vapor-cell MOT was constructed. The vapor cell was pumped by an ion pump down to a typical pressure 10^{-9} Torr. The two external-cavity diode lasers were used for cooling and repumping the rubidium atoms. The cooling laser was tuned to 15 MHz below the $5S_{1/2}$ $(F=3)$–$5S_{3/2}$ $(F=4)$ atomic transition and the repumping laser was resonant with the $5S_{1/2}$ $(F=2)$–$5P_{3/2}$ $(F=3)$ transition. The cooling laser beam has a diameter of 16 mm and an intensity of 1.2 mW/cm^2, and the repumping laser beam has a diameter of 16 mm and an intensity of 0.4 mW/cm^2.

A typical diameter of the atomic cloud in the MOT was about 1 mm, and the number of atoms trapped therein was about 10^7. According to the time-of-flight (TOF) measurement, the temperature of the atomic cloud in the MOT was about 150 μK. The number of atoms guided by the HLB was detected by observing the fluorescence excited by a horizontally placed probe laser beam tuned to the resonance of the atomic transition $5S_{1/2}$ $(F=3)$–$5P_{3/2}$ $(F=4)$. The probe laser beam has a cross section of 1 mm height and 10 mm width and was positioned at 110 mm below the center of the MOT. An additional laser beam overlapping the probe laser beam was used for the optical repumping of atoms. The repumping laser beam was at resonance with the transition $5S_{1/2}$ $(F=2)$–$5P_{3/2}$ $(F=3)$.

The procedure of preparing cold atoms for atom guiding includes two basic stages, trapping atoms in the MOT and cooling atoms down to a typical temperature of 20 μK by the polarization gradient cooling (PGC) technique. The PGC procedure included the following steps: (i) first, the anti-Helmholtz magnetic field of the MOT was quickly switched off; (ii) after a 5-ms delay, the detuning of the cooling laser was increased from -15 MHz to -70 MHz; (iii) in 5 ms, the intensity of the cooling laser was decreased to a one-third value of the initial intensity.

After the PGC procedure, the cooling and repumping laser beams were blocked by the mechanical shutters, and simultaneously the HLB was introduced into the atomic cloud by opening another mechanical shutter. Then, the atoms started falling into the HLB due to gravitation.

VIII. GUIDING EFFICIENCY: EXPERIMENTAL RESULTS AND NUMERICAL SIMULATIONS

According to our experimental setup, the detected atomic flux depends on two basic processes, atom loading from the optical molasses into the HLB and atom guiding in the HLB. To characterize the first process, we introduce the loading efficiency η_l determined as the ratio of the number of atoms loaded into the HLB (N_{load}) to the initial number of atoms in the optical molasses (N_{in}),

$$\eta_l=\frac{N_{load}}{N_{in}}. \tag{40}$$

According to the definition, the loading efficiency depends mainly on the relation between the initial size of the atomic cloud characterized by radius r_{in} and the size of the ring-shaped potential barrier of the HLB described by radius r_{HLB}.

The second process is described by the guiding efficiency η_g defined as the ratio of the number of atoms in the guided atomic flux (N_{guide}) to the number of atoms loaded into the HLB (N_{load}),

$$\eta_g=\frac{N_{guide}}{N_{load}}. \tag{41}$$

This guiding efficiency depends mainly on the intensity and the detuning of the HLB, and the initial temperature of atoms before guiding. It can also depend on the background pressure in the vacuum chamber. Under our experimental conditions, the influence of the background pressure on the guiding efficiency could be practically neglected at a pressure of about 10^{-9} Torr.

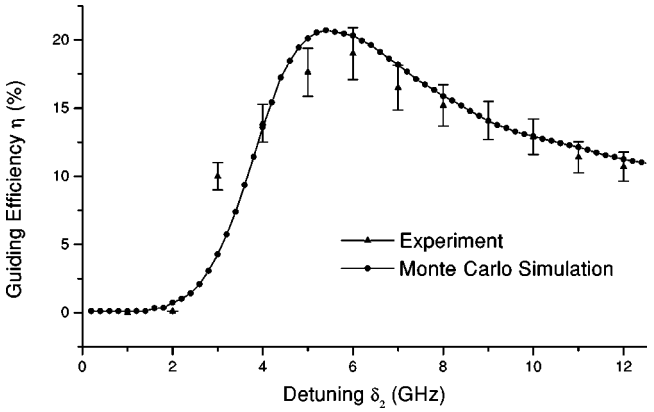

FIG. 4. The guiding efficiency as a function of the detuning δ_2. The initial atomic temperature is $T=20$ μK. The power of the HLB is 180 mW and the maximum intensity of the HLB at the MOT position is 500 mW/cm^2.

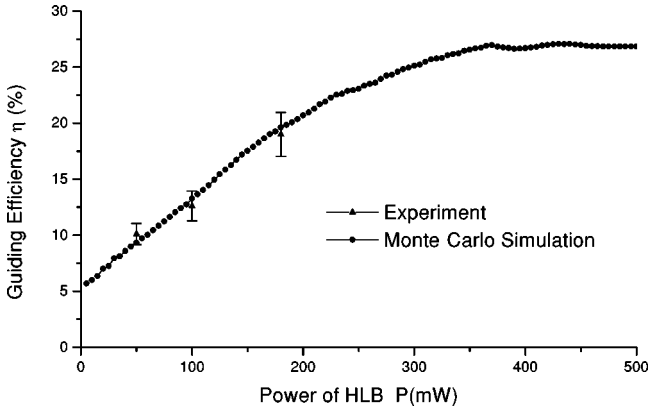

FIG. 5. The guiding efficiency as a function of the HLB power at the atomic temperature of $T=20$ μK and detuning $\delta_2=6$ GHz.

In order to get high loading efficiency, r_{HLB} should be larger than r_{in}. However, when r_{HLB} is increased, the height of the potential barrier is decreased due to the decrease in the effective saturation parameter, which then decreases the guiding efficiency. The efficient transfer of atoms from the MOT to the observation region is thus possible under some optimal conditions. In our experiment, the loading efficiency was typically in the range of $\eta_l=70$–90%, depending on the initial atomic temperature and the parameters of the atom-HLB interaction.

Figure 4 shows the experimental dependence of the guiding efficiency on the detuning $\delta_2=\omega-\omega_2$ (refer to Fig. 1). For comparison, Fig. 4 also shows the dependence obtained by the Monte Carlo simulation based on the forces, diffusion tensor, and optical potential presented in Sec. V. The maximum guiding efficiency, about 20%, is observed at the detuning $\delta_2=6$ GHz. The guiding efficiency decreases sharply at smaller detunings due to the destructive contribution of the radiation pressure force.

At small detunings, the radiation pressure force becomes important. The force decelerates the atoms and reverses the velocities of the slowly moving atoms, reducing finally the guided atomic flux and accordingly the guiding efficiency. The slight discrepancy between the experimental and computational results may arise mainly for the following main reasons: (i) the limited detection efficiency of the TOF method did not allow us to detect slowly moving atoms due to the large time delay of the TOF signal, (ii) the contribution of the radiation pressure force could be higher than that estimated by a simple three-level interaction model. At about 3 GHz detuning, the HLB was close to a resonance and accordingly increased the efficiency of optical repumping, which could also produce an additional error in the detection process.

Figure 5 shows the dependence of the guiding efficiency on the power of the HLB at a fixed detuning. The guiding efficiency increases with the power due to the increase of the potential barrier. At a high laser power, the guiding efficiency saturates or even decreases. This is another manifestation of the contribution of the radiation pressure force that was directed opposite to the guiding direction in our experimental scheme. The radiation pressure force then reduced the guiding efficiency as explained before.

Figure 6 shows the dependence of the guiding efficiency on the initial temperature of the atomic cloud. We found that when the temperature was lower than 30 μK, the guiding efficiency rose dramatically, especially at temperatures below 10 μK. That dependence is in good correspondence with the temperature dependence of the Boltzmann factor.

Figures 5 and 6 allow us to compare two possible ways of increasing the guiding efficiency, by increasing the power of the HLB or by decreasing the temperature of the atomic cloud. Our experimental results show that a 30% guiding efficiency can be attained at the initial temperature of 10 μK if the power of the HLB is only 180 mW, while at the initial temperature of 20 μK, the required power is as much as 500 mW. From an experimental point of view, the decrease in temperature by 10 μK is much easier than the threefold increase in the laser power.

In Fig. 7 we finally compare the guiding efficiencies for the two possible HLB-propagation directions, with respect to the guiding direction. The Monte Carlo simulations show that the efficiency of atomic guiding in the copropagating HLB is generally higher than in the counterpropagating HLB, due to the opposite role of the radiation pressure force. While the radiation pressure force prevents slow atoms from reaching the observation region in the counterpropagating

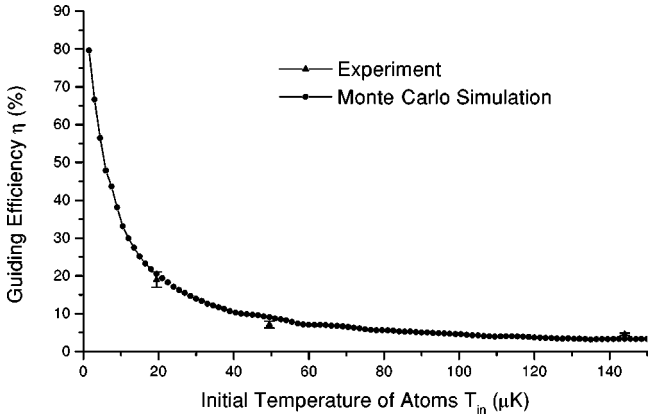

FIG. 6. The guiding efficiency as a function of the initial atomic temperature at the HLB power of $P=180$ mW and detuning $\delta_2=6$ GHz.

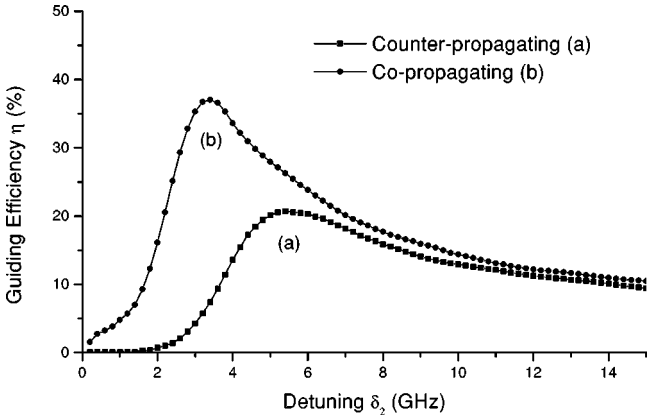

FIG. 7. The guiding efficiency as a function of the detuning: (a) when the HLB propagates counter to the direction of atom guiding, and (b) when the HLB propagates in the direction of atom guiding. The HLB power is $P=180$ mW and the initial temperature is $T=20$ μK.

case, it pushes all the atoms into the observation region in a co-propagating case, thus increasing the guiding efficiency.

IX. CONCLUSION

We have guided the cold ^{85}Rb atoms in the HLB over a distance of 11 cm with a maximum guiding efficiency about 20%. We have also developed a simple model of atomic guiding for a three-level dipole-interaction scheme. The experimental results are in good agreement with the Monte Carlo simulations based on the three-level model. We also found that the guiding efficiency depends strongly on the intensity and the detuning of the HLB and the initial temperature of atoms.

The experimental results show that the guiding efficiency is influenced strongly by the radiation pressure force at small detunings. The Monte Carlo simulations prove that the guiding efficiency as a function of detuning depends on the direction of the atomic propagation with respect to that of the HLB. When the atoms and the HLB propagate counter to each other, the maximum guiding efficiency is observed at a large detuning value. On the other hand, when the atoms propagate in the direction of the HLB, the maximum guiding efficiency shifts to a small detuning. We also found that a small decrease in the initial temperature sharply increases the guiding efficiency, while the same increase in the guiding efficiency needs much more HLB power.

ACKNOWLEDGMENTS

We would like to thank Dr. W.D. Phillips for stimulating discussions. We are also grateful to J.P. Yin and Y. Lin for their contributions to the initial stage of the experiment. This work was supported by the Creative Research Initiatives of the Korean Ministry of Science and Technology. Y.W. is grateful to the National Science Foundation of China (Contract No. 19834060) and the Ministry of Science and Technology (95-Yu-34) for financial support.

APPENDIX

Below are listed the steady-state populations $r_{11}^0, r_{22}^0, r_{33}^0$ and coherences c_1, s_1, c_2, s_2 for a three-level Λ atom in the field of a laser beam of Eq. (2) [23]:

$$r_{11}^0=\frac{L_2(2\mu_1+L_1)}{2\Delta},\quad r_{22}^0=\frac{L_1(2\mu_2+L_2)}{2\Delta},\quad r_{33}^0=\frac{L_1L_2}{2\Delta},$$

$$c_1=s_{13}^0+s_{31}^0=-\frac{2u_1(\delta_1-\mathbf{k}\cdot\mathbf{v})}{\gamma^2+(\delta_1-\mathbf{k}\cdot\mathbf{v})^2}\frac{\mu_1L_2}{\Delta},$$

$$s_1=i(s_{13}^0-s_{31}^0)=\frac{2\gamma u_1}{\gamma^2+(\delta_1-\mathbf{k}\cdot\mathbf{v})^2}\frac{\mu_1L_2}{\Delta},$$

$$c_2=s_{23}^0+s_{32}^0=-\frac{2u_2(\delta_2-\mathbf{k}\cdot\mathbf{v})}{\gamma^2+(\delta_2-\mathbf{k}\cdot\mathbf{v})^2}\frac{\mu_2L_1}{\Delta},$$

$$s_2=i(s_{23}^0-s_{32}^0)=\frac{2\gamma u_2}{\gamma^2+(\delta_2-\mathbf{k}\cdot\mathbf{v})^2}\frac{\mu_2L_1}{\Delta},$$

where the common denominator is given by

$$\Delta=\mu_1L_2+\mu_2L_1+3L_1L_2/2,$$

and all other quantities are determined by Eqs. (5), (16), and (17).

[1] R. Cook and R. Hill, Opt. Commun. **43**, 258 (1982).
[2] M. A. Ol'Shanii, Yu. B. Ovchinnikov, and V. S. Letokhov, Opt. Commun. **98**, 77 (1993).
[3] S. Marksteiner, C. M. Savage, P. Zoller, and S. L. Rolston, Phys. Rev. A **50**, 2680 (1994).
[4] W. Jhe, M. Ohtsu, H. Hori, and S. R. Friberg, Jpn. J. Appl. Phys., Part 2 **33**, L1680 (1994).
[5] M. J. Renn, D. Montgomery, O. Vdovin, D. Z. Anderson, C. E. Wieman, and E. A. Cornell, Phys. Rev. Lett. **75**, 3253 (1995).
[6] H. Ito, K. Sakaki, T. Nakata, W. Jhe, and M. Ohtsu, Opt. Commun. **115**, 57 (1995).
[7] M. J. Renn, E. A. Donley, E. A. Cornell, C. E. Wieman, and D. Z. Anderson, Phys. Rev. A **53**, R648 (1996).
[8] V. I. Balykin, D. V. Laryushin, M. V. Subbotin, and V. S. Letokhov, JETP Lett. **63**, 802 (1996).
[9] H. Ito, T. Nakata, K. Sakaki, M. Ohtsu, K. I. Lee, and W. Jhe, Phys. Rev. Lett. **76**, 4500 (1996).
[10] M. J. Renn, A. A. Zozulya, E. A. Donley, E. A. Cornell, and D. Z. Anderson, Phys. Rev. A **55**, 3684 (1997).
[11] H. Ito, K. Sakaki, M. Ohtsu, and W. Jhe, Appl. Phys. Lett. **70**, 2496 (1997).
[12] M. V. Subbotin, V. I. Balykin, D. V. Laryushin, and V. S. Letokhov, Opt. Lett. **139**, 107 (1997).
[13] T. Kuga, Y. Torii, N. Shiokawa, T. Hirano, Y. Shimizu, and H. Sasada, Phys. Rev. Lett. **78**, 4713 (1997).
[14] Yu. B. Ovchinnikov, I. Manek, and R. Grimm, Phys. Rev. Lett. **79**, 2225 (1997).
[15] O. Morsch and D. R. Meacher, Opt. Commun. **148**, 49 (1998).

[16] S. Kuppens, M. Rauner, M. Schiffer, K. Sengstock, W. Ertmer, F. E. van Dorsselaer, and G. Nienhaus, Phys. Rev. A **58**, 3068 (1998).
[17] J. Yin, H. Noh, K. Lee, K. Kim, Y. Wang, and W. Jhe, Opt. Commun. **138**, 287 (1997).
[18] J. Yin, Yifu Zhu, and Y. Wang, Phys. Rev. A **57**, 1957 (1998).
[19] J. Yin, Y. Zhu, W. Jhe, and Yuzhu Wang, Phys. Rev. A **58**, 509 (1998).
[20] J. Yin, Y. Zhu, W. Wang, Y. Wang, and W. Jhe, J. Opt. Soc. Am. B **15**, 25 (1998).
[21] K. I. Lee, Ph. D. thesis, Seoul National University, 1999 (unpublished).
[22] C. Cohen-Tannoudji, J. Dupont-Roc, and G. Grynberg, *Atom-Photon Interactons, Basic Processes and Applications (*Wiley, New York, 1992).
[23] V.G. Minogin and V.S. Letokhov, *Laser Light Pressure on Atoms* (Gordon and Breach, New York, 1987).